Chapter-II
Materials and Experimental Techniques

Abstract

This chapter deals with the discussion about synthesis of polymer and organometallic compound by chemical method. The brief working principles and operation of Cyclotron and Pelletron accelerators have been discussed. Different characterization techniques have been used to do off-line analysis of the pristine and irradiated samples to study the ion beam induced modification of the composites. The specifications of these techniques are discussed in this chapter.

2.0 Introduction

This chapter deals with the description of the material (polymer and filler) used for the present study, the working principle of accelerators and various techniques used for offline measurement of pristine and irradiated samples. Detail description of following is considered in this chapter.

- Materials: Properties and preparation methods of Polymer/Fillers
- Working principle and specifications of Pelletron and Cyclotron accelerators
- Sample and Target preparation for irradiation, Thickness measurement
- Calculation of ion range and its energy loss using SRIM code
- AC electric response
- Vicker's Microhardness
- X-ray Diffraction
- Fourier Transform Infra-red (FTIR) Spectroscopy
- Atomic Force Microscopy (AFM)
- Scanning Electron Microscopy (SEM)
- Differential Scanning Calorimetry (DSC)
- UV-Vis Spectroscopy
- Superconducting Quantum Interference Device (SQUID)

2.1 Materials

2.1.1 Polymethyl methacrylate (PMMA)

PMMA is an amorphous, transparent and colourless thermoplastic which is hard and stiff but brittle and notch-sensitive. The industrial production of PMMA precursors started as early as 1907. The methyl methacrylate monomers are produced from natural oil by several routes.

PMMA undergoes bond cleavage both in the main chain and side chains upon ion irradiation. The first effect leads to decrease in the average molar mass and the second effect leads to the formation of volatile reaction products such as C_2H_4, CO_2 and CO[1]. Section 1.5 (Chapter-1) describes the motivation of selecting PMMA as a matrix material of composites for present study.

(i) Synthesis:

Polymethyl methacrylate (PMMA) was synthesized by solution polymerization method. In this procedure, a monomer is dissolved in a non-reactive solvent that contains a catalyst. The heat released by the reaction is absorbed by the solvent and so the reaction rate is reduced. The complete process for PMMA synthesis is described below.

The benzoyl peroxide (BPO:0.8 g an initiator for polymerization) was dissolved in fresh inhibitor-free 80 ml methyl methacrylate monomer with ethyl acetate as a solvent (80 ml) in a round bottom flask. This solution was properly refluxed for about 5 h at 80 °C temperature in the hot water bath. The resulting solution was precipitated out in another beaker containing methanol (100 ml). The precipitated PMMA was allowed to dry at room temperature [2].

(ii) Properties of PMMA

Molecular formula: $[-C_5O_2H_8-]_n$

Chemical structure:

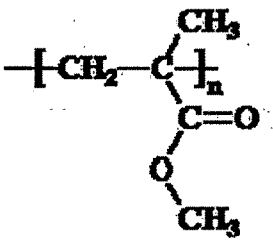

Polymer Type: Thermoplastic

Density (g cm^{-3}): 1.19

Refractive index: 1.49

Dielectric constant @ 1 MHz: 2.6

Dissipation factor @ 1 MHz: 0.014

Heat deflection temperature: <100 °C

Melting point: 130-140 °C

Glass Transition Temperature: ~110 °C

Solubility: Acetone, Tetrahydrofuran

Advantages: Excellent clarity and UV resistance. Good abrasion resistance, hardness and stiffness. Low water absorption, low smoke emission, good track and arc resistance.

Applications: It can be used to prepare lenses, light covers, glazing (particularly in aircraft), light pipes, meter covers, bathroom fittings, outdoor signs, baths, toys etc. Acrylic film is laminated over ABS sheet to provide UV protection.

2.1.2 Polyimide(PI)

Polyimides are high temperature engineering polymers originally developed by the DuPont Company. Polyimides are a very interesting group of incredibly strong and astoundingly heat and chemical resistant polymers.

(i) Properties of PI:

Chemical Structure:

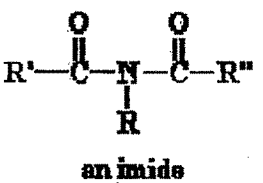

an imide

Polymer type: Thermoplastic polymer

Density (g/cm^3): 1.42

Refractive index: 1.66

Dielectric Constant 1MHz: 3.4

Dissipation Factor 1 kHz: 0.0018

Heat deflection Temperature: 300°C

Melting Temperature: >400 °C*

(* Generally, PI deform before the temperature reaches to its melting point)

Glass Transition Temperature: 385 °C

Advantages: When compared to most other organic or polymeric materials, polyimides exhibit an exceptional combination of thermal stability (>500°C), mechanical toughness and chemical resistance.

Disadvantages: Disadvantages of polyimide includes high cost, a low flammability and higher moisture absorption. One of the major disadvantages of polyimides is the high degree of dielectric anisotropy due to chain alignment near the substrate.

Applications: They are used in the construction of many appliances as well as microwave cookware and food packaging because of their thermal stability, resistance to oils, greases, and fats, and their transparency to microwave radiation. They can also be used in circuit boards, insulation and fibre for protective clothing, composites and adhesives. These polymers have such incredible mechanical and thermal properties that they are used in place of metals and glasses in many high performance applications in the electronics, automotive, and even the aerospace industries. For present work, commercial grade polyimide film was taken.

2.1.3 Fillers

(i) Ferric Oxalate (Fo)

Synthesis:

It was formed by taking 6.24g of oxalic acid and 5.24g of ferric chloride with ethanol as a solvent in a round bottom flask, and it was refluxed for 4h at 60 ^{0}C. The excess of ethanol was then distilled out and the substance was dried at 75 ^{0}C for 3h in an oven [2].

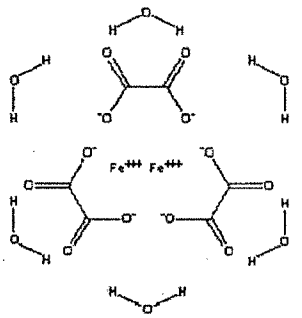

Properties of Fo:

Formula: $Fe_2(C_2O_4)_3$

Appearance: Pale yellow-green

Molecular weight: 375.7 g/mole

Melting point: 150°C

Solubility: Soluble in organic solvent, alcohol

(ii) Palladium actylacetonate [Pd(acac)]

Commercially available Palladium actylacetonate [Pd(acac)] of Sigma-Aldrich Inc., US and was provided by IUAC, New Delhi.

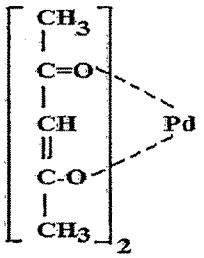

Properties of Pd(acac):

Formula: $Pd(CH_3COCHCOCH_3)_2$

Appearance: Yellow crystalline powder

Molecular weight: 304.62 g/mole

Melting point: 205°C

Solubility: Soluble in organic solvent, alcohol, insoluble in water

(iii) Ni-Dimethylglyoxime (Ni-DMG)

The organometallic compound nickel dimethylglyoxime (Ni-DMG) was formed by dissolving

0.4 mole nickel chloride in 200 ml water and it was heated at 80 °C; a slight excess of the alcoholic dimethylglyoxime was added and then dilute ammonia solution was added drop wise with continuous stirring until precipitation takes place. The precipitate was then washed with cold water until free from Cl^- and dried at 110 °C for 1 h [3].

Properties of Ni-DMG

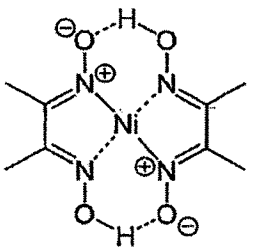

Formula: Ni ($C_4H_7O_2N_2$)

Appearance: Red crystalline powder

Molecular weight: 173.8 g/mole

Melting point: 250 °C

Solubility: Soluble in organic solvent, alcohol

Not soluble in water, ammonia

(iv) Ni Powder

Commercially available Ni metal powder of Laborchemikalein was taken.

Properties of Ni powder:

Appearance: Gray-black powder

Atomic weight: 58.69 g/cm^3

Melting point: 1455 °C

2.1.4 Polymer composites

Polymer composites were prepared by doping different concentrations i.e. 5, 10, 15 wt.% of Ferric oxalate and Ni-DMG; 10, 20, 30, 40 wt.% of Pd(acac) and Ni powder in PMMA with acetone and toluene as a solvent. The mixture of polymer and filler was stirred for 2-3 hours and then pour in to a clean glass trough. Thus the composite films were prepared by casting method.

2.1.5 Thin film preparation using RF Sputtering

In present work thin film of metal/polymer was prepared by RF co-sputtering. Direct current methods can't be used to sputter insulating targets due to the build-up of positively charged sputtering gas ions which repel the bombarding (sputtering) ions. This difficulty can be overcome by using radio frequency (RF) sputtering. In RF sputtering a high frequency alternating potential is used to neutralize surface charges

periodically. RF sputtering apparatus can be used to deposit conducting, semiconducting and insulating films.

Description of Sputtering Unit

Sputtering is a technology in which the material is released from the source at much lower temperature than evaporation. The substrate is placed in a vacuum chamber with the source material, named a target and an inert gas (such as argon) is introduced at low pressure. Gas plasma is struck using an RF power source, causing the gas to become ionized. The ions are accelerated towards the surface of the target, causing atoms of the source material to break off from the target in vapor form and condense on all surfaces including the substrate.

A schematic diagram of a typical RF sputtering system is shown in the Fig. 2.1. RF sputtering unit has been indigenously developed [4] at NSC for thin film deposition. It consists of three parts: Sputtering chamber and the vacuum system, the gas flow system and the RF system with matching network.

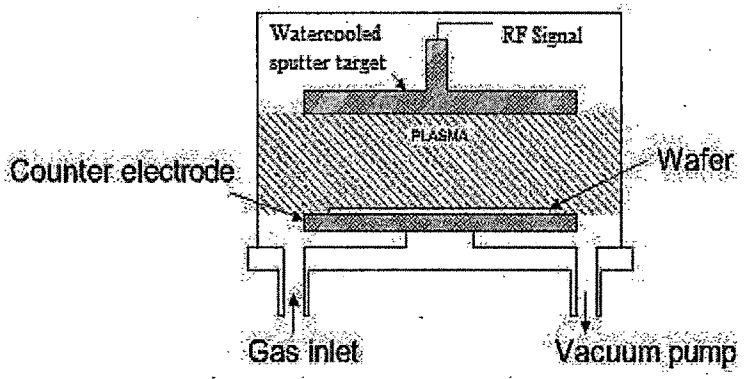

Figure 2.1 Schematic of Sputtering Unit

The sputtering chamber is made of stainless steel having a diameter of 40 cm. It contains a target holder acting as cathode (10 cm diameter) and a substrate holder acting as anode. Substrates are kept on the anode at a distance of 5 cm from the cathode. This distance is chosen in a manner such that enough number of collisions should take place in the gaseous medium for an operating pressure of ~$5x10^{-2}$ to $7x10^{-2}$ Torr. The cathode is connected to the RF power supply. The anode and the rest of the system are properly grounded with metallic strips. The substrate holder is kept on an electrically insulated height adjustable table. To evacuate this chamber, a diffusion pump (500 l/c) based high vacuum system is used. A rotary pump (200 l/m) is used for backing the diffusion pump as well as to rough the sputtering chamber. An ultimate base pressure of $2x10^{-6}$ Torr is obtained. The target holder is a metal holder fitted with a Teflon ring. The metal holder has water connections in order to cool the target. The Teflon ring contains circular rubber gasket which is fitted into the grooves of the ring. A proper RF shielding is made in the sides of cathode to check the spread of plasma in unwanted direction inside the chamber and to maximize the plasma within cathode and anode [5].

In present case, the Fe doped PI films were prepared on glass and silicon substrate by RF sputtering. Using RBS measurement the weight concentration of Fe in the composite was found to be 0.5, 1 and 5%. These films were irradiated with 120 MeV Ni^{10+} beam at the fluence of $5x10^{12}$ ions/cm^2 to study its surface, magnetic and optical properties. The results are presented in Chapter-4.

2.1.6 Thickness measurement of the composite films

The thickness of chemically synthesized composites was measured by a sensitive digital instrument. Sensitivity of the instrument was 0.001 mm. The thickness of the polymers was measured at 7-8 places chosen randomly and average of it was taken.

The obtained thicknesses are listed in Table 2.1. Thickness of PI+Fe thin film was measured by elipsometry method and was confirmed by RBS results.

Table 2.1: Thickness of the polymers

Sample	Thickness
Pure PMMA films	150 μm
PMMA+Fo film	120 μm
PMMA+Pd(acac)	170 μm
PMMA+Ni-DMG	150 μm
PMMA+Ni Powder	70 μm
PI+Fe	100 nm

2.2 Ion beam irradiation

2.2.1 Accelerators

Energetic ions for polymer irradiation can be produced in several ways. Now a days the most common approach is the use of ion implanters or ion accelerators. The basic difference between both machines is, on the one hand, the available energy range and on the other, the ion beam currents delivered from each device. Ion implanters usually work in the range of 10 to several 100 keV energy interval delivering high currents that can go from tens of μA to tens of mA. Ion accelerators work in the MeV energy region but with lower currents that in extreme cases can reach the 100μA.

Present work deals with two types of high energetic charge particle accelerators.

(i) Cyclotron accelerator

(ii) Pelletron accelerator

Following section covers the brief discussion about the principle and functionality of these accelerators.

(i) Cyclotron accelerator

The concept of cyclotron was originated in 1929 by the late E.O. Lawrence and the first cyclotron was built by M. S. Livingston in 1931. The cyclotron may be considered as a linear accelerator which has been wrapped up into a flat spiral, housed in an evacuated chamber with the addition of a steady magnetic field perpendicular to its plane.

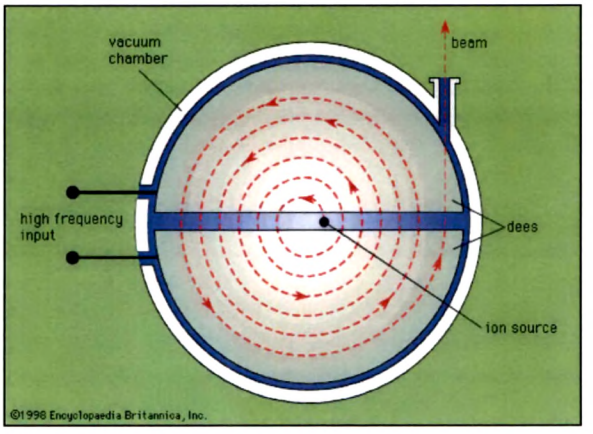

Fig. 2.2 Schematic representation of Cyclotron accelerator

Cyclotron consists of two dees which are driven by an alternating voltage of fixed frequency. A positive ion released from a centrally located ion source between the dees is acted on by the electric field in between them, being attracted towards whichever dees is negatively charged. The magnetic field is applied perpendicular to the path of the ions which keeps them in circular path. The accelerating high frequency field is applied to the gaps only, whereas the dees remain field free. As the particles traverse each semicycle in the same time, independent of their velocity, the high frequency field at the gap can be constant unless relativistic effect starts playing a role. In this case suitable modelling of the magnetic field has to be done to maintain

the cycling phase. As the magnetic field keeps them in a semicircle, the interelectrode gap is reached and dees potential polarity has reversed, this leads to the second acceleration of the ions. As the particle path radius increases with the square root of the particle energy, the total particle trajectory becomes a spiral. That is, the beam has to be injected near the centre of the Dees and it is fed out of the cyclotron at its maximum radius.

For present work, the 3 MeV Proton irradiation on polymeric samples was performed by Cyclotron at Punjab University, Chandigarh. This machine is adapted and built out of the components of the Variable Energy Cyclotron at the University of Rochester, Rochester, New York, USA. It is a single Dee classical cyclotron with arrangement for variable frequencies from 10 to 20 MHz and a main magnetic field upto a maximum of 14 kGauss. This permits the variability of the energy of the various accelerated ions. Beams of 1-5 MeV proton, 4 MeV deuteron, 1-2 MeV and 7-8 MeV alpha and up to 11 MeV He^{3++} have been obtained at the target. The pressure is maintained ~$5x10^{-6}$ mm Hg in whole vacuum system. Total power of 110 kW is required when the machine is fully operative with all the accessories. The operational characteristics and the general features of the cyclotron are discussed below [7].

1.	Maximum magnetic field	14 K Gauss
2.	Maximum Power consumption in Magnet	40 KVA (400 Amp at 100 V)
3.	Weight of the magnet	20 tons
4.	Size of the pole pieces	26 inches
5.	Gap distance between the pole pieces	6 5/16 inches
6.	Frequency range of the oscillator	10 MHz to 20 MHz
7.	Maximum power of the oscillator	25 KVA
8.	Dee voltage	30-40 KV

9.	Dee size	25 inches dia
10.	Ion source	Hooded arc type
11.	Vacuum	$5x10^{-6}$ mm of Hg
12.	Distance of the analysing magnet from the chamber	12 ft
13.	Distance of the target from the analysing magnet	18 ft
14.	Internal beam	15 microamperes
15.	External beam	1.5-2 microamperes
16.	Analysed beam	0.5 microamperes
17.	Attainable energies of particles	
	(i) Protons 2-8 MeV	
	(ii) Deuterons 1-4 MeV	
	(iii) Alphas 2-8 MeV	
	(iv) He^3 2-11 MeV	
18.	Total power consumption	100 KVA

(ii) Pelletron accelerator

The model 15 UD Pelletron is a tandem electrostatic accelerator capable of accelerating any ion from proton to uranium up to the energy of 200 MeV depending on the ion. This electrostatic accelerator at IUAC is installed with a vertical configuration in an insulating tank which is 26.5 m long and 5.5m in diameter and filled up with SF_6 as an insulating gas (Fig. 2.3). Inside this tank, there is a high voltage terminal. This terminal can be charged to a high potential that can be varied from 4 to 15 MV. This terminal is connected to the tank vertically through ceramic titanium tubes called accelerating tubes. A potential gradient is maintained through these tubes from high voltage to ground from top of the tank to the terminal as well as

from terminal to the bottom of the tank. Negative ions from the ion source are injected in to the accelerator and accelerated towards the terminal. The negative ion source system, consisting of a high negative potential deck, three ion sources, vacuum systems, power supplies and controls for the sources is used to produce ions for injection into the accelerator. Ions from all the elements in the periodic tables can be produced with variety of ion sources. The terminal also has an offset quadrupole triplet lens with a variable aperture and Faraday cup to select the desired charge state after stripping.

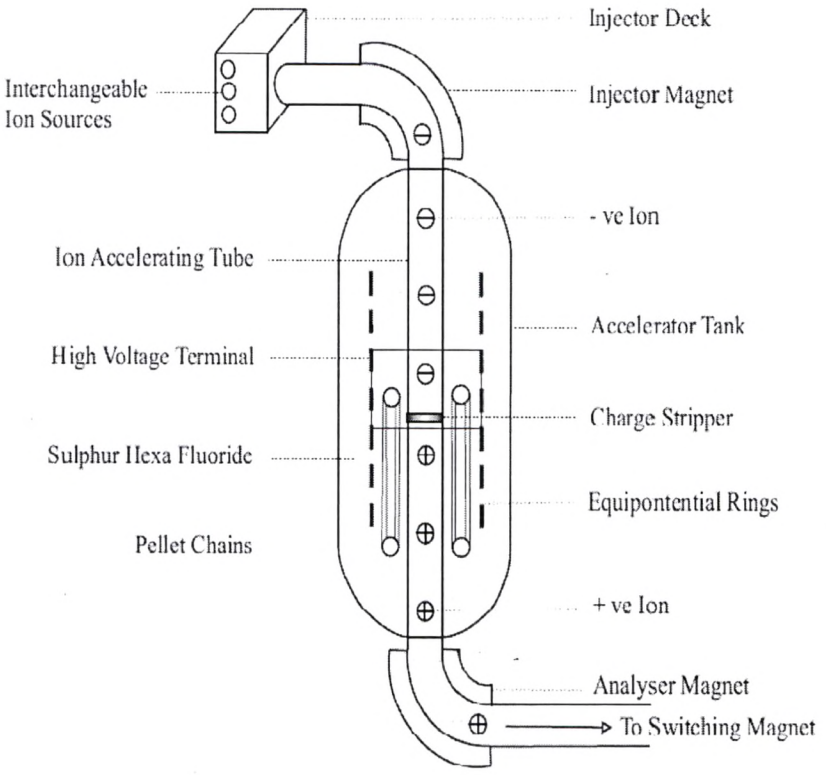

Fig. 2.3 Schematic representation of working principle of pelletron

In the terminal the negative ions are stripped off few electrons and thereby converted to positive ions, which are further accelerated as they proceed to the bottom of the

tank at ground potential. As a result the ions emerging out of the accelerator gain energy given by $E = V(q + 1)$ MeV.

where V is the terminal potential (in MV) and q is the number of positive charges on the ion after stripping. These high energy ions are then analysed to the required energy with the help of a 90^{o} bending magnet known as analyser magnet, and directed to the desired experimental area with the help of a multiport switching magnet which can deflect the beam into any of the seven beam lines in the beam hall [8]. The irradiation of the samples was carried out in scattering chamber of material science beam line (Fig. 2.4).

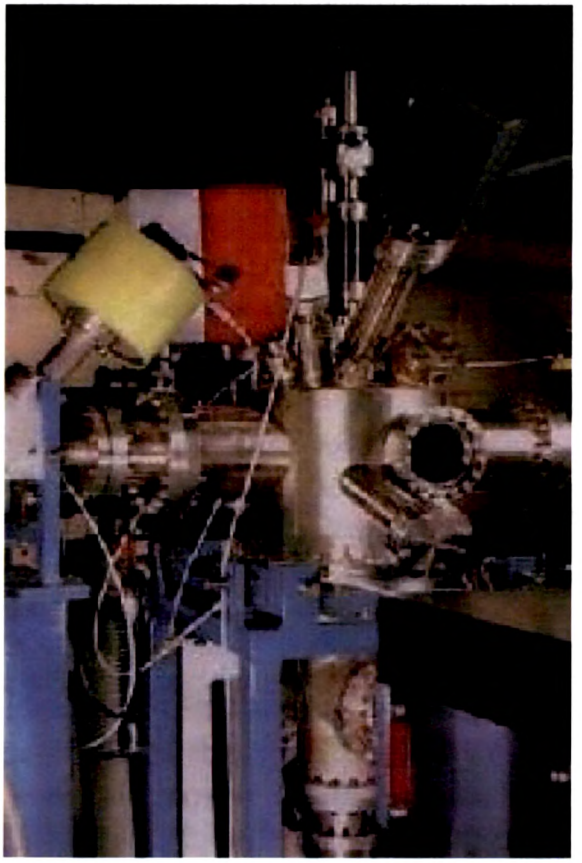

Fig. 2.4 Material Science Irradiation Chamber at IUAC, New Delhi

Fluence estimation

The ion fluence was estimated by time of irradiation and beam current as follow,

$$I = \frac{Q}{T} = \frac{Dqe}{T} = \frac{\phi Aqe}{T}$$

$$\therefore T = \frac{\phi Aqe}{I}$$

Where, I = ion current (nA)

Q= total charge

D= dose = ion fluence (φ) in ions/cm^2 x area (A) of irradiation in cm^{-2}

q= charge state

e= electronic charge = 1.6x10^{-19} C

T= Time of irradiation (Sec)

Since, the number of particles per nano ampere of beam current = $\frac{I}{qe}$(pnA)

$$\therefore T = \frac{\phi A}{beam\ \ current\ \ (pnA)}$$

Using above equation, the required time for each fluence was calculated. During experiment, keeping current of the ion beam constant, the sample was irradiated for the pre-determined time for a particular fluence.

2.2.2 Calculation of range and energy loss by SRIM code

SRIM is a group of programs which calculate the stopping and range of ions (up to 2 GeV/amu) into a matter using a quantum mechanical treatment of ion-atom collisions (assuming a moving atom as an "ion", and all target atoms as "atoms"). This calculation is made very efficient by the use of statistical algorithms which allow the ion to make jumps between calculated collisions and then averaging the collision

results over the intervening gap. During the collisions, the ion and atom have a screened Coulomb collision, including exchange and correlation interactions between the overlapping electron shells. The ion has long range interactions creating electron excitations and plasmons within the target. These are described by including a description of the target's collective electronic structure and interatomic bond structure when the calculation is setup. The charge state of the ion within the target is described using the concept of effective charge, which includes a velocity dependent charge state and long range screening due to the collective electron sea of the target.

The particle's energy is reduced after each free-flight path by the amount of electronic energy loss and then (after the collision) by the so-called nuclear energy loss which is the result of transferring momentum to the target atom in the collision. Each ion's history is terminated either when the energy drops below a pre-specified value or when the particle has moved out of the front or rear surface of the target.

Thus SRIM code can be used to calculate the ion distribution and for quick calculation of damage, detailed calculation with full damage cascades, calculation of surface sputtering, Electron/ Neutron/Photon cascades, various ion energy/angle/positions, special multilayers biological targets, stopping power for ions in gases and the stopping of ions in compounds.

In the present work we have calculated the projected range, nuclear stopping power and electronic stopping power of 3 MeV proton, 120 MeV Ni^{10+} and 140 MeV Ag^{11+} ions in PMMA and 120 MeV Ni^{10+} ions in PI using code SRIM 2003 [6].

Results obtained by SRIM-2003 code

When energetic charged ion strikes a polymeric target, it loses its energy by two mechanisms known as electronic and nuclear stopping. The projected range of 3 MeV proton beam in PMMA was calculated to be 126 μm. The electronic stopping power

$(dE/dX)_e$ of the beam is 1.418 eV/Å and nuclear stopping power $(dE/dX)_n$ of the beam is $8.879x10^{-4}$ eV/ Å.

The projected range of 120 MeV Ni^{10+} beam in PMMA was found to be 29 μm. The electronic stopping power $(dE/dX)_e$ is $5.39x10^2$ eV/Å whereas nuclear stopping power $(dE/dX)_n$ is $7.67x\ 10^{-1}$ eV/ Å.

The projected range of 140 MeV Ag^{11+} beam in PMMA was found to be 24 μm. The electronic stopping power $(dE/dX)_e$ is $9.57x10^2$ eV/Å whereas nuclear stopping power $(dE/dX)_n$ is 2.92 eV/Å.

In all the cases, maximum energy of the ion beam was lost by electronic interactions. The thickness of the polymer is larger than the projected range of the beam in the polymer. Hence the beam was stopped in the polymer and maximum dissipation of heat took place at the end. The composite shows a lower projected range due to increase in density after doping filler.

When Polyimide was irradiated with 120 MeV Ni^{10+} ion beam, the projected range of the beam is about 27 μm which is quite high as compared to film thickness (~100 nm). Electronic stopping power was obtained to be $5.89x10^2$ eV/Å while nuclear stopping power is $8.25x10^{-1}$ eV/Å. This implies that most of energy loss was due to electronic energy loss and beam penetrates through the sample.

2.2.3 Irradiation

The samples were irradiated with 3 MeV proton beam at the fluences of $5x10^{12}$ and $1x10^{13}$ ions/cm^2 using Cyclotron of Punjab University, Chandigarh; 120 MeV Ni^{10+} ions and 140 MeV Ag^{11+} ions at the fluences of $1x10^{11}$ and $5x10^{12}$ ions/cm^2 using Pelletron Accelerator, Inter University Accelerator Centre, New Delhi. Both irradiations were carried out at an ambient temperature. Following Table 2.2 shows the irradiation details of different samples.

Table 2.2 Irradiation details of the samples

Sr. No	Sample (polymer)	Fluence (ions/cm^2)	Current density nA/cm^2	Energy and Ions
1.	Pure PMMA	$5x10^{12}$, $1x10^{13}$	20	3 MeV Proton
	PMMA+5%Fo	$5x10^{12}$, $1x10^{13}$	20	3 MeV Proton
	PMMA+10% Fo	$5x10^{12}$, $1x10^{13}$	20	3 MeV Proton
	PMMA+15% Fo	$5x10^{12}$, $1x10^{13}$	20	3 MeV Proton
2.	PMMA+10% Pd(acac)	$5x10^{12}$, $1x10^{13}$	20	3 MeV Proton
	PMMA+20% Pd(acac)	$5x10^{12}$, $1x10^{13}$	20	3 MeV Proton
	PMMA+30% Pd(acac)	$5x10^{12}$, $1x10^{13}$	20	3 MeV Proton
	PMMA+40% Pd(acac)	$5x10^{12}$, $1x10^{13}$	20	3 MeV Proton
3.	PMMA+5%Ni-DMG	$5x10^{12}$, $1x10^{13}$	20	3 MeV Proton
	PMMA+10% Ni-DMG	$5x10^{12}$, $1x10^{13}$	20	3 MeV Proton
	PMMA+15% Ni-DMG	$5x10^{12}$, $1x10^{13}$	20	3 MeV Proton
4.	PMMA+10% Ni	$5x10^{13}$	20	3 MeV Proton
	PMMA+20% Ni	$5x10^{13}$	20	3 MeV Proton
	PMMA+30% Ni	$5x10^{13}$	20	3 MeV Proton
	PMMA+40% Ni	$5x10^{12}$	20	3 MeV Proton
5.	Pure PMMA	$1x10^{11}$, $5x10^{12}$	5	120 MeV Ni^{10+}
	PMMA+5% Fo	$1x10^{11}$, $5x10^{12}$	5	120 MeV Ni^{10+}

	PMMA+10% Fo	$1x10^{11}$, $5x10^{12}$	5	120 MeV Ni^{10+}
	PMMA+15% Fo	$1x10^{11}$, $5x10^{12}$	5	120 MeV Ni^{10+}
6.	PMMA+10% Pd(acac)	$1x10^{11}$, $5x10^{12}$	5	120 MeV Ni^{10+}
	PMMA+30% Pd(acac)	$1x10^{11}$, $5x10^{12}$	5	120 MeV Ni^{10+}
	PMMA+40% Pd(acac)	$1x10^{11}$, $5x10^{12}$	5	120 MeV Ni^{10+}
7.	PMMA+10% Ni	$5x10^{12}$	5	120 MeV Ni^{10+}
	PMMA+20% Ni	$5x10^{12}$	5	120 MeV Ni^{10+}
	PMMA+40% Ni	$5x10^{12}$	5	120 MeV Ni^{10+}
8.	Polyimide (PI)	$5x10^{12}$	5	120 MeV Ni^{10+}
	PI+0.5%Fe	$5x10^{12}$	5	120 MeV Ni^{10+}
	PI+1%Fe	$5x10^{12}$	5	120 MeV Ni^{10+}
	PI+5%Fe	$5x10^{12}$	5	120 MeV Ni^{10+}
9.	Pure PMMA	$1x10^{11}$, $5x10^{12}$	5	140 MeV Ag^{11+}
	PMMA+5% Fo	$1x10^{11}$, $5x10^{12}$	5	140 MeV Ag^{11+}
	PMMA+10% Fo	$1x10^{11}$, $5x10^{12}$	5	140 MeV Ag^{11+}
	PMMA+15% Fo	$1x10^{11}$, $5x10^{12}$	5	140 MeV Ag^{11+}
10.	PMMA+10% Pd(acac)	$1x10^{11}$, $5x10^{12}$	5	140 MeV Ag^{11+}
	PMMA+30% Pd(acac)	$1x10^{11}$, $5x10^{12}$	5	140 MeV Ag^{11+}
	PMMA+40% Pd(acac)	$1x10^{11}$, $5x10^{12}$	5	140 MeV Ag^{11+}

2.3 Characterization techniques

The pristine and irradiated samples were analysed with different characterization techniques to study their physical, chemical, structural, thermal properties and surface morphology. Different characterization techniques with their working principle and specifications have been discussed in following subsections.

2.3.1 Dielectric properties (LCR meter/Impedance gain-phase Analyser)

Generally the atoms of polymer have their electrons, tightly bound to the central long chain and side groups through 'covalent' bonding. Covalent bonding makes it much more difficult for most conventional polymers to support the movement of electrons and therefore they act as insulators.

In general, the chemical bonds between unlike atoms in polymer molecules possess permanent electric dipole moments. Many polymers have chemical structure such that the bond moments can vectorially accumulate into molecular or segmental moments in many molecular configurations or conformations. These polymers can therefore by virtue of these moments be polarized by an electric field. They are said to be "dielectrically active", i.e. they show polarization due to orientation of permanent dipoles. The measurement of the polarization induced in dielectrically active polymers has proven to be an extremely useful method for probing polymer structure.

Generally, Dielectric constant is an ability of the material to store electric charge through polarization. Reasonably straightforward formulas have been derived from statistical mechanics and electrostatics that connect the magnitude of the induced equilibrium polarization with microscopic quantities such as the number and magnitude of dipole moment and the energy of interaction between moments. Thus it

is often possible to deduce quantitative molecular information from dielectric measurements. The molecular motions in a given polymer tend to have a very broad range of relaxation times at constant temperature and are thermally activated, often with large activation energies; the capability of broad frequency range of measurement is very important consideration [9].

Figure 2.5 shows Impedance gain-phase analyser/LCR meter, available at M. S. University of Baroda, Vadodara. This Impedance/Gain-Phase analyser (Solartron-1260) uses powerful microprocessor-controlled digital and analogue techniques to provide a comprehensive range of impedance and frequency response measuring facility. It can be operated for the frequency range from 10 Hz to 30 MHz. Dielectric loss, capacitance and resistance were obtained directly from LCR meter. Using the values of capacitance and dielectric loss, dielectric constant and ac electrical conductivity were calculated at an ambient temperature in the frequency range of 100 Hz to 10 MHz for pristine and irradiated samples.

Fig. 2.5 Impedance gain/phase analyser (Solartron 1260)

(i) AC electrical conductivity

It is the reciprocal of resistivity, most often expressed in terms of S/m. where S is the reciprocal of ohm is siemens, abbreviated as S. Free electrons which are present in the polymer structure but not attached to the macromolecular chain structure of polymer,

contribute to the conductivity of polymer. Though they are very less in number, so the conductivity of the thermoplastic polymers like PMMA, PVC, PI etc are obtained to be very less. In present study we have reported two effective techniques to improve conductivity of the polymer by several order (i) By dopping metal/organometallic compound in polymer: In this case conductivity depends on the size, shape and amount of filler (ii) By ion beam irradiation: In this case conductivity depends on ion specie, fluence and its energy. Conductivity measurement is again an important issue. Composite material was inserted between two electrodes. The sample holder is shown in Fig. 2.5. The a.c. conductivity has been determined as follows.

A capacitor when charged under an a.c. voltage will have some loss in current due to ohmic resistance or impedance by heat absorption. If Q is the charge in Coulomb due to a potential difference of V volts between two plates of a condenser of area A, and interplate distance t, then a.c. conductivity ($\sigma_{a.c.}$) due to a.c. voltage V is given by the relation.

$$\sigma_{a.c.} = \frac{J}{E} \tag{2.3.1}$$

Where J is the current density and E the electrical field strength vector which is $E = D/\varepsilon$; D being the displacement vector of the dipole charges and ε is the complex permittivity of the material. For a parallel plate capacitor the electric field intensity (E) is the ratio of the potential difference between the plates of the capacitor to the interplate distance i.e.

$$E = \frac{V}{t} \tag{2.3.2}$$

Since $\frac{Q}{A} = \frac{V\varepsilon}{t}$, the current density $J = \frac{dq}{dT}$ is given by

where $q = \frac{Q}{A}$ and $\frac{d}{dT}$ is differentiation w.r.t. time

$$J = \frac{dq}{dT} = \frac{d}{dT}\left(\frac{V\varepsilon}{t}\right) = \frac{\varepsilon}{t}\frac{dV}{dT} \tag{2.3.3}$$

$$J = \frac{\varepsilon}{d} V j\omega \tag{2.3.4}$$

Substituting for E and J in eq. (2.3.1),

$$\sigma_{a.c.} = \frac{J}{E} = \varepsilon j\omega$$

$$= (\varepsilon - j\varepsilon'')j\omega = \varepsilon j\omega + \omega\varepsilon'' \tag{2.3.5}$$

For the a.c. conductivity to be a real quantity, the term containing j has to be neglected, hence

$$\sigma_{a.c.} = \omega\varepsilon'' \tag{2.3.6}$$

In any dielectric material, there will be some power loss because of the work done to overcome the frictional damping forces encountered by the dipoles during their rotation. If an a.c. field is considered, then in an ideal case the charging current I_c will be 90° out of phase with the voltage. But in most of the capacitors due to the absorption of electrical energy some loss current, I_L will also be produced, which will be in phase with the voltage. Charging current I_c and loss current I_L will make angles δ and θ respectively with the total current I, passing through the capacitor. The loss current is represented by sinδ of the total current I.

Generally sinδ is called the loss factor but when t is small, the sinδ= δ= tanδ.

$$\varepsilon'(\omega) = D_o \cos(\delta/E_o) \tag{2.3.7}$$

$$\varepsilon''(\omega) = D_o \sin(\delta/E_o) \tag{2.3.8}$$

Since the displacement vector (D_o) in a time varying field will not be in phase with E and hence there will be a phase difference d between them. From eq. (2.3.7) and (2.3.8), we have

$$\tan\delta = \frac{\varepsilon''(\omega)}{\varepsilon'(\omega)} \qquad (2.3.9)$$

Substituting the value of ε"(ω) from eq. (2.3.9) in to eq. (2.3.6), we have

$$\sigma_{a.c.} = \omega\varepsilon(\omega)\tan\delta \qquad (2.3.10)$$

Where ω =2πf and ε= $\varepsilon_o\varepsilon_r$, ($\varepsilon_r$ is the relative permittivity of the material and ε_o the permittivity of free space).

Therefore

$$\sigma_{ac.} = 2\pi f \tan\delta\ \varepsilon_o\varepsilon_r \qquad (2.3.11)$$

Dielectric constant or relative permittivity can be calculated by using the formula

$$\varepsilon_r = \frac{C_p \times t}{\varepsilon_o A} \qquad (2.3.12)$$

From equation (2.3.11) and (2.3.12) one can get the relation,

$$\sigma_{a.c.} = \frac{2\pi f \tan\delta C_p t}{A} = \frac{2\pi f C_p D t}{A} \qquad (2.3.13)$$

Eq. (2.3.13) has been used to calculate the a.c. conductivity of the polymer.

where, D (dissipation factor) = tanδ, which is measured directly from LCR meter. C_p: Capacitance of the dielectric at given frequency. A and t are the area of the electrode and thickness of the sample respectively.

(ii)Dielectric Constant

Dielectric constant can be defined by, (a) The property of a dielectric which determines the electrostatic energy stored per unit volume for unit potential. (b) The ratio of the capacity of a condenser having a dielectric material between the plates to that of the same condenser when the dielectric is replaced by a vacuum.

Therefore ε = C_p / C_0, where C_p is capacitance measured using the impedance gain-phase analyser; C_0= ε_0 A/t, where ε_0 is the permittivity of free space, A is the cross-

sectional area of the electrode and t is the thickness of the polymeric film. It is also known as Permittivity and Specific inductive capacity.

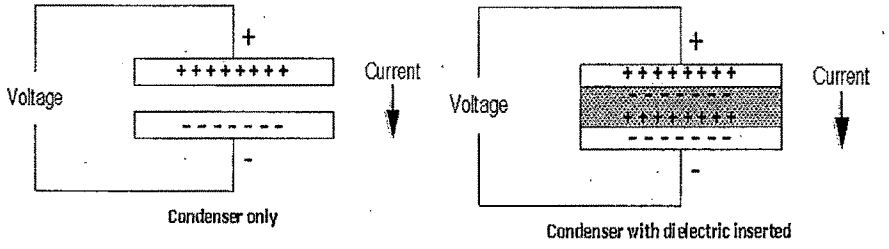

Fig. 2.6 Polarization in dielectric material

When dielectric material is inserted between the plates, which already contain surface charge, the effect of the dielectric field is to induce polarization in the material in such a way that the material remains neutral but induced charge appears on the plates in addition to the original ones as shown in Fig. 2.6.

The insertion of a dielectric between the plates of, say, a parallel-plate capacitor always increases its capacitance, or ability. As the dielectric constant increases, the electric flux density increases, if all other factors remain unchanged. This enables objects of a given size, such as sets of metal plates, to hold their electric charge for long periods of time, and/or to hold large quantities of charge. Materials with high dielectric constants are useful in the manufacture of high-value capacitors.

A vacuum capacitor with an electric field E between its metallic plates has an interfacial charge $Q_o=\varepsilon_o E$, where $\varepsilon_o = = 8.854 \times 10^{-12}$ F/m is the dielectric permittivity of free space. If the field E varies with temperature, the charge Q_o also follows it. If the capacitor is filled with a material medium-gaseous, liquid or solid, the charge induced is increased by the polarization P of the medium, so

$$Q = Q_o + P = \varepsilon_o(1+\chi)E = \varepsilon \qquad (2.3.14)$$

where ε is the permittivity and χ the susceptibility of the dielectric medium. The dielectric constant, ε, of the sample was computed using the formula

$$\varepsilon = \frac{C_p}{C_o} \tag{2.3.15}$$

where C_p is the measured capacitance and $C_o = \varepsilon_o A/t$, where ε_o is the permittivity of free space (8.854×10^{-12} F/m), A is area of the electrode and t is thickness of the sample.

(iii) Dissipation factor/Dielectric loss/ tanδ

It is a measure of the hysteresis in charging and discharging a dielectric. Loss tangent, a synonym for dissipation factor, is a quantification of loss in the capacitor. The loss tangent is the tangent of the phase angle relationship between capacitor voltage and capacitor current as the angle departs from the theoretical 90 degree value as a result of loss mechanisms within the capacitor. δ is also known as the loss angle. It can also define as a measure of loss-rate of power of a mechanical mode, such as an oscillation, in a dissipative system. For example, electric power is lost in all dielectric materials, usually in the form of heat. It was measured directly from LCR meter.

2.3.2 Vicker's Microhardness

Organic polymers are inherently soft due to the absence of chemical bonds between polymer chains. Hardness is important solid state property to characterize such material. Hardness of a solid may be broadly defined as its ability to resist penetration by another harder solid [10].

The general definition of indentation hardness which is related to various forms of indenters is the ratio of applied load to the surface area of indentations [11, 12].

Fig. 2.7 Vicker's Microhardness Indenter Future Tech. (FM-700)

Hardness of a material depends upon a large number of factors such as impurities, dislocations, vacancies, temperature, composition, etc., which control growth and structure of crystals.

The determination of hardness of a material is normally made using a mechanical test that gives a measure of ease with which the material can be locally deformed. Hardness can be determined by various tests such as scratch test, abrasion test, plowing test, rebound test, cutting test, damping test, erosion test and indentation test [13].

Most hardness testers produce plastic deformation in materials and they all are based on microscopic indentations made using appropriate loads. The size of the impression of indentation is related to the applied load and the yield stress of the material [14].

The load effect of microhardness is an important phenomenon, which needs to be thoroughly investigated to obtain information relating to the laws governing mechanical properties of materials. The hardness results mostly follow Hays and Kendall's law [15-18].

Hardness measurements have been used to investigate the materials response to irradiation since elastic properties and hardness are related to crosslink number density [19] and can be measured accurately and conveniently [20, 21]. Hardness of

the irradiated sample depends on the beam parameters like ion specie, energy and fluence.

When polymeric materials are subjected to high energy ion beams, a high number density of crosslinks is introduced as well as numerous double and triple bonds and free radicals are formed. As a consequence, irradiation process makes polymer harder. During the experiment smooth and clean surface was subjected to indentation test at room temperature using Vickers microhardness tester (Future Tech. Corp., Japan FM-700) as shown in Fig. 2.7, attached to a Carl Zeiss's Axiotech microscope. Loads ranging from 100 to 1000 mN were used for making indentations, keeping the time of indentation constant as 30 seconds in all cases. The diagonal lengths of indentation marks were measured using a micrometer eyepiece at proper magnification and averages of these diagonal lengths were recorded. Hardness being the ratio of load applied to the surface area of indentation, which for a Vickers diamond pyramid indenter, is represented by the equation [22],

$$H_v = \frac{2P\sin{\alpha/2}}{d^2} = 1.854 \times P/d^2 \qquad (2.3.16)$$

where H_v is the Vickers hardness number, P is the applied load in mN, d in μm is the average diagonal length of the indentation mark and α is the angle between two opposite faces, which is 136° for Vickers hardness.

During the process of indentation, the indenter penetrates a depth comparable with or greater than the thickness of the distorted zone. Consequently, a noticeable increase in H_v is observed in the beginning. As the depth of the impression of diamond pyramid increases, the influence of the distorted zone becomes less significant. This explains that there is almost no variation of H_v at higher load.

2.3.3 X-ray Diffraction

X-rays are electromagnetic radiation of wavelength about 1 Å (10^{-10} m), which is about the same size as an atom. X-ray diffraction has been in use in two main areas, for the fingerprint characterization of crystalline materials and the determination of their structure. Each crystalline solid has its unique characteristic X-ray powder pattern which may be used as a "fingerprint" for its identification. Once the material is identified, X-ray crystallography may be used to determine its structure, i.e. how the atoms pack together in the crystalline state and what the interatomic distance and angle etc. X-ray diffraction is one of the most important characterization tools used in solid state chemistry and materials science.

The phenomenon of X-ray diffraction by material forms a scattering process in which the X-rays are scattered by the electrons of the atoms without change in wavelength. A diffracted beam is produced by such scattering only when certain geometric conditions are satisfied. The resulting diffraction pattern of a crystal, comprising both the positions and intensities of the diffraction effects, is a fundamental physical property of the substance, serving not only for its speedy identification but also for the complete explanation of its structure. Analysis of the positions of the diffraction effects leads immediately to a knowledge of the size, shape and orientation of the unit cell. To locate the positions of the individual atoms in the cell, the intensities must be measured and analysed [23].

Instrumentation: X-ray diffractometers consist of three basic elements: an X-ray tube, a sample holder, and an X-ray detector.

X-rays are generated in a cathode ray tube by heating a filament to produce electrons, accelerating the electrons towards a target by applying a voltage and bombarding the

target material with electrons. When electrons have sufficient energy to dislodge inner shell electrons of the target material, characteristic X-ray spectra are produced.

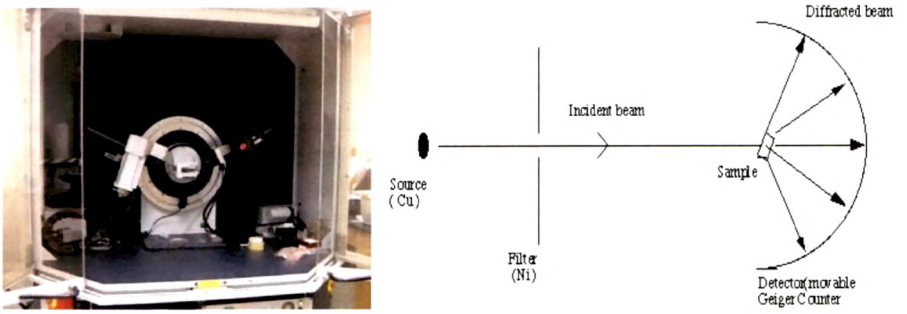

Fig. 2.8 Shimadzu's X-ray Diffractometer and diffraction phenomenon

These spectra consist of several components, the most common being K_α and K_β. K_α consists, in part, of $K_{\alpha 1}$ and $K_{\alpha 2}$. $K_{\alpha 1}$ has a slightly shorter wavelength and twice the intensity as $K_{\alpha 2}$. The specific wavelengths are characteristic of the target material (Cu, Fe, Mo, Cr). Filtering, by foils or crystal monochrometers, is required to produce monochromatic X-rays needed for diffraction. $K_{\alpha 1}$ and $K_{\alpha 2}$ are sufficiently close in wavelength such that the average of the two is used. Copper is the most common target material for single-crystal diffraction, with CuK_α radiation = 1.5418Å. These X-rays are collimated and directed onto the sample as shown in Fig. 2.8. As the sample and detector are rotated, the intensity of the reflected X-rays is recorded. When the geometry of the incident X-rays impinging the sample satisfies the Bragg equation, constructive interference occurs and a peak in intensity occurs. A detector records and processes this X-ray signal and converts the signal to a count rate which is then output to a device such as a printer or computer monitor. Routinely, a 2θ range of 5 to 70 degrees is sufficient to cover the most useful part of the powder pattern. The scanning speed of the counter is usually 2θ of 1degree/min and therefore, about 60 minutes are needed to obtain a trace.

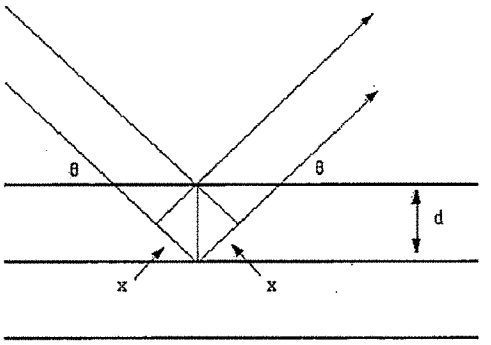

Fig. 2.9 Reflection of X-rays from two planes of atoms in a solid

Fig. 2.9 shows the schematic representation of diffraction of X-rays from two layers. The condition for diffracted beam is given by the relation,

$$n\lambda = 2d \sin \theta \qquad (2.3.17)$$

where n is an integer- the order of reflection, d the interplaner spacing between successive atomic planes in the crystal, λ is the wavelength of the X-rays and θ is the angle between the atomic plane and both the incident and reflected beams. This fundamental relation is known as the Bragg equation or Bragg law.

Crystallite-size determination

Scherrer [24] first showed that the mean dimension, D, of the crystallites is related to the pure X-ray diffraction broadening *l* by the equation,

$$D = \frac{K\lambda}{l\cos\theta} \qquad (2.3.18)$$

where K is constant approximately equal to unity and related to the crystalline shape, *l* is FWHM of the diffraction peak.

Percentage crystallintiy of the composites was determined by area ratio method. In this method the areas of amorphous and crystalline parts of the pattern were calculated.

In present work the structural studies were carried out by X-ray powder diffractometer (model: Shimadzu, XRD-6000/Bruker's X-ray Diffraction-D8) with Cu K_α radiation (1.5418 Å) for a Bragg angle $5^\circ \leq 2\theta \leq 60^\circ$ at the scanning rate of 1 degree/min.

2.3.4 FTIR Spectroscopy

FT-IR stands for Fourier Transform InfraRed, the preferred method of infrared spectroscopy. In infrared spectroscopy, IR radiation is passed through a sample. Some of the infrared radiation is absorbed by the sample and some of it is passed through (transmitted). The resulting spectrum represents the molecular absorption and transmission, creating a molecular fingerprint of the sample. Like a fingerprint, no two unique molecular structures produce the same infrared spectrum. This makes infrared spectroscopy useful for several types of analysis.

Fourier Transform Infrared (FT-IR) spectrometry was developed in order to overcome the limitations encountered with dispersive instruments. The main difficulty was the slow scanning process. A method for measuring all of the infrared frequencies simultaneously, rather than individually, was needed. A solution was developed which employed a very simple optical device called an interferometer. The interferometer produces a unique type of signal which has all of the infrared frequencies "encoded" into it. The signal can be measured very quickly, usually on the order of one second or so. Thus, the time element per sample is reduced to a matter of a few seconds rather than several minutes. The signal coming from interferometer is called interferogram with all frequencies simultaneously. Thus, the use of interferometer results in extremely fast measurements. Because the analysis requires a frequency spectrum (a plot of the intensity at each individual frequency) in order to make identification, the measured interferogram signal can not be interpreted directly. A means of "decoding" the individual frequencies is required. This can be

accomplished via a well-known mathematical technique called the Fourier transformation. This transformation is performed by the computer which then presents the user with the desired spectral information for analysis.

When an interferogram is Fourier transformed, a single beam spectrum is generated. A single beam spectrum is a plot of raw detector response versus wavenumber. A single beam spectrum obtained without a sample is called a background spectrum, which is induced by the instrument and the environments. Characteristic bands around 3500 cm^{-1} and 1630 cm^{-1} are ascribed to atmospheric water vapour and the bands at 2350 cm^{-1} and 667 cm^{-1} are attributed to carbon dioxide. A background spectrum must always be run when analyzing samples by FTIR. When an interferogram is measured with a sample and Fourier transformed, a sample single beam spectrum is obtained. It looks similar to the background spectrum except that the sample peaks are superimposed upon the instrumental and atmospheric contributions to the spectrum. To eliminate these contributions, the sample single beam spectrum must be normalized against the background spectrum. Consequently, a transmittance spectrum is obtained as follows.

$$\%T = \frac{Intensity\ of\ sample\ beam}{Intensity\ of\ reference\ beam} \times 100 = \frac{I}{I_o} \times 100 \qquad (2.3.19)$$

Where $\%T$ is transmittance; I is the intensity measured with a sample in the beam (from the sample single beam spectrum); I_o is the intensity measured from the back ground spectrum

The absorbance spectrum can be calculated from the transmittance spectrum using the following equation.

$$A = -log_{10}T \qquad (2.3.20)$$

where A is the absorbance.

The final transmittance/absorbance spectrum should be devoid of all instrumental and environmental contributions and only present the features of the sample. If the concentrations of gases such as water vapour and carbon dioxide in the instrument are the same when the background and sample spectra are obtained, their contributions to the spectrum will ratio out exactly and their bands will not occur. If the concentrations of these gases are different when the background and sample spectra are obtained, their bands will appear in the sample spectrum [25].

Fig. 2.10 Thermo-Nicolet NEXUS 670

Fig. 2.10 shows Thermo-Nicolet NEXUS 670 FTIR spectrometer which measures spectrum in the frequency range of 510 – 4000 cm^{-1} with a resolution of 4 cm^{-1}. FTIR spectroscopy does not require a vacuum, since neither oxygen nor nitrogen absorbs infrared rays. FTIR analysis can be applied to minute quantities of materials, whether solid, liquid, or gaseous. When the library of FTIR spectral patterns does not provide an acceptable match, individual peaks in the FTIR plot may be used to yield partial information about the specimen.

2.3.5 Surface Morphology

(i) Atomic force microscopy(AFM)

Atomic force microscopy is a basic technique and inevitable for all nanoscopic research. The atomic force microscope (AFM) is a very high-resolution type of scanning probe microscope. MFM is one of the foremost tools for the manipulation of matter at the nanoscale. Figure 2.11 represents the AFM instrument and its working principle.

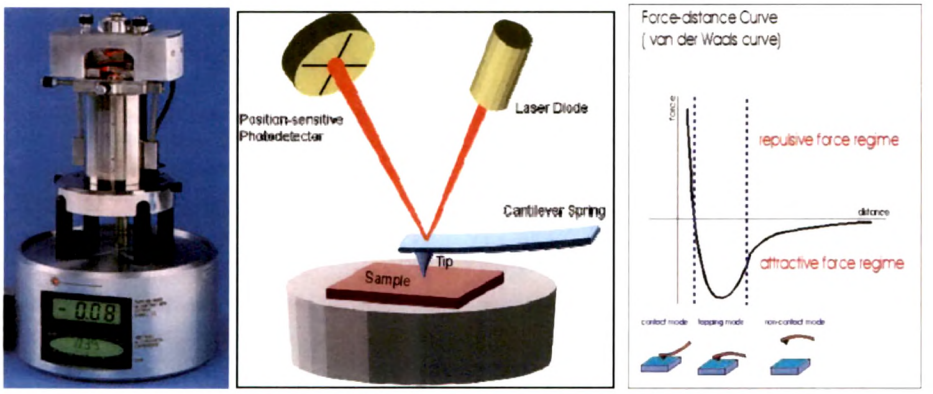

Fig. 2.11 Instrumentation and working principle of AFM

The AFM consists of a cantilever (probe) with a sharp tip at its end that is used to scan the specimen surface. The AFM tips are usually micro-fabricated silicon cones or silicon nitride four-sided pyramids, the latter with high durability, that are commercially available mounted to cantilevers with spring constant of 0.05-1.5 N/m for contact AFM and 40-80 N/m for tapping mode AFM. These tips are not solid but hollow, which improves their performance. When the tip is brought into close proximity of a sample surface, the Van der Waals force between the tip and the sample leads to a deflection of the cantilever according to Hooke's law. Typically, the deflection is measured using a laser spot reflected from the top of the cantilever into an array of photodiodes. However a laser detection system can be expensive and

bulky; an alternative method in determining cantilever deflection is by using piezoresistive AFM probes. These probes are fabricated with piezoresistive elements that act as a strain gauge. Using a Wheatstone bridge, strain in the AFM probe due to deflection can be measured, but this method is not as sensitive as laser deflection.

If the tip was scanned at a constant height, there would be a risk that the tip would collide with the surface, causing damage. Hence, in most cases a feedback mechanism is employed to adjust the tip-to-sample distance to maintain a constant force between the tip and the sample. Generally, the sample is mounted on a piezoelectric tube, that can move the sample in the z direction for maintaining a constant force and the x and y directions for scanning the sample. The resulting map of $s(x,y)$ represents the topography of the sample.

Over the years additional modes of operation have been developed for the AFM. The primary modes of operation are contact mode, non-contact mode, and dynamic contact mode.

Roughness on pristine and irradiated polymer surfaces is certainly of enormous practical importance for polymer applications. Surface roughening due to irradiation sometimes play important role in adhesion of functional coatings. However, there is a tendency to neglect the topology at the expense of phase imaging. Generally, tapping-mode AFM is less reliable with topology, but it is frequently preferred as phase contrast can be recorded that is usually applied for determining physical and chemical differences in composites [26-28].

For present surface study, Digital Nanoscope IIIa Instrument Inc. is used in tapping mode at IUAC, New Delhi and Nanoscope-E, Digital Instrument from USA in contact mode at IUC Indore. Both instruments contain silicon nitride tip attached at the end of

cantilever with length about 100 μm and having 0.5 N/m spring constant. Average surface roughness was determined using this instrument.

(ii) Scanning electron microscopy (SEM)

The scanning electron microscope (SEM) is a type of electron microscope capable of producing high-resolution images of a sample surface. Due to the manner in which the image is created, SEM images have a characteristic three-dimensional appearance and are useful for judging the surface structure of the sample.

The Scanning electron microscope and its operation is shown in Fig. 2.12. The two major parts are the microscope column and the electronics console. The microscope column consists of the electron gun, one or two condenser lenses, two pairs of beam deflection coils, the objective lens and some apertures. In the specimen chamber at the lower end of the microscope column are located the specimen stage and the detectors are located for the deflection of different signals generated by the electron-specimen interaction.

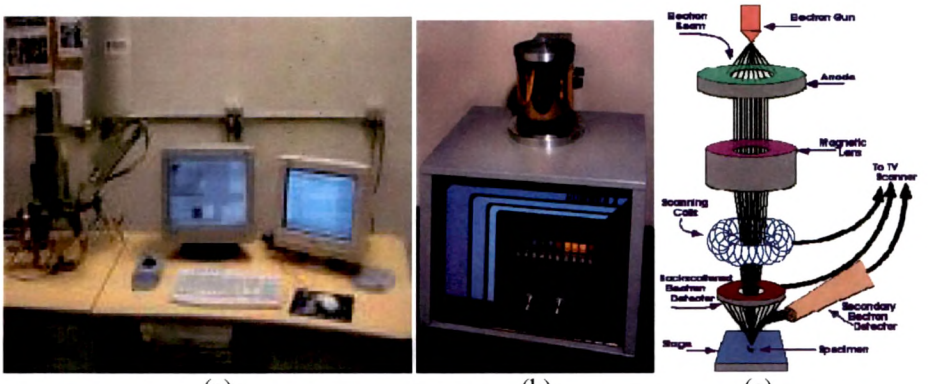

(a) (b) (c)

Fig. 2.12 (a) SEM unit (b) coating unit (c) working principle

The microscope column and the specimen chamber are evacuated using a combination of prevacuum and high vacuum pumps. The pressure in the specimen chamber typically amounts to about 10^{-4} Pa, allowing the beam electrons to travel

from the cathode to the specimen with little interaction with the residual gas molecules. The electronics console consists of the electric power supplies of the acceleration voltage (~0.5-30 kV) as well as the condenser and objective lenses, the scan generator, the electronic amplifiers for the different signals acquired. Modern SEM mostly uses a PC to control the electron beam, to select the signals and to record as well as to store the digital images [29].

Sample Preparation: Because the SEM utilizes vacuum conditions and uses electrons to form an image, special preparations must be done to the sample. Water must be removed from the samples because the water would vaporize in the vacuum. All metals are conductive and require no preparation before being used. All non-metals need to be made conductive by covering the sample with a thin layer of conductive material. This is done by using a device called a "sputter coater" shown in Fig 2.12(b). The working principle of SEM is shown in figure 2.12(c). The electron beams are emitted from the cathode and accelerated by a voltage of 0.5 to 30 kV between the cathode and anode forming a smallest beam cross section near the anode with a diameter of about 10-50μm. This spot size is too large to produce a sharp image. Therefore the crossover is demagnified by the lens system consisting of one or two condenser lenses and one objective lens and focused on the specimen surface. Most SEMs can produce an electron beam having a smallest spot size of about 5-10 nm and an electron probe current in the range of 10^{-12} to 10^{-10} A, which is sufficient to form an image with a reasonable signal to noise ratio. The objective lens has a variable, relatively long focal length that allows a large working distance (distance between the specimen and lower pole piece) in the range of about 5-30 mm. The signal generated by the impinging beam (Fig. 2.12) collected by detectors located lateral above the specimen with sufficient efficiency [29].

For present work, scanning electron microscopy (SEM) Model: JEOL JSM 5600 at FCIPT, Gandhinager and Oxford_INCA energy dispersive X-ray spectrometer at ERDA, Vadodara have been used. The study of surface topography of pristine and irradiated samples were done at different magnification i.e. 500x to 2000x.

2.3.6 Differential Scanning Calorimetry (DSC)

Differential scanning calorimetry measures temperature and heat flows associated with thermal transitions in a material. DSC monitors heat effects associated with phase transitions and chemical reactions as a function of temperature. In DSC, the energy difference between the sample and the reference is measured [30]. General schematic of DSC apparatus is shown in Fig. 2.13.

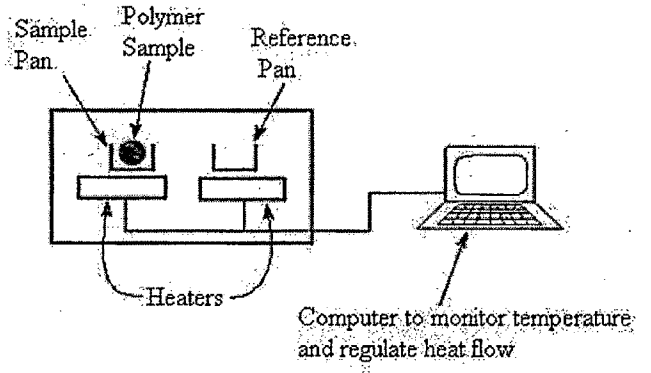

Fig. 2.13 Schematic diagram for the working principle of DSC

There are two pans. One is the sample pan, where sample is kept. The other one is the reference pan which is empty. Each pan sits on top of a heater. Commands are given to computer which allows the heater to turn on and heat both the pans at a specific rate, usually ~ 10 °C per minute. The polymer sample means there is extra material in the sample pan. Having extra material means that it will take more heat to keep the temperatures of the sample pan increasing at the same rate as the reference pan. So the heater underneath the sample pan has to work harder than the heater underneath the

reference pan. It has to put out more heat. By measuring just how much more heat it has to put out is what we measure in a DSC experiment.

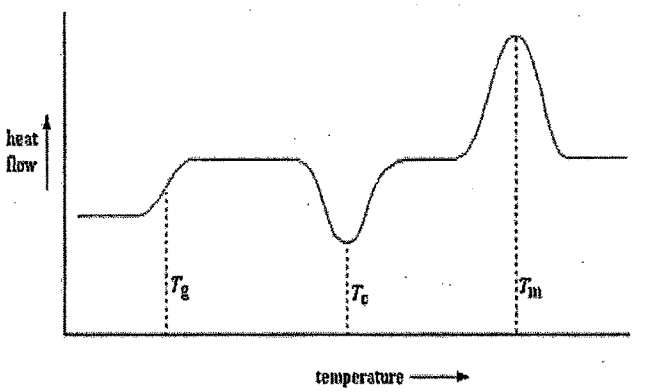

Fig. 2.14 Different phenomenon taking place during DSC measurement

When we start heating two pans, the computer will plot the difference in heat output of the two heaters against temperature. The plot gives information about glass transition, critical and melting temperature of the material as shown in figure 2.14.

The Glass Transition Temperature: After a certain temperature, plot will shift upward suddenly. This means that the heat capacity of polymer has increased because the polymer has just gone through the glass transition. It is known that polymers have a higher heat capacity above the glass transition temperature than they do below it. To measure this glass transition temperature, DSC can be used.

Crystallization: Above the glass transition, the polymers have a lot of mobility. They wiggle and squirm, and never stay in one position for very long. When they reach the right temperature, they will have gained enough energy to move into very ordered arrangements, which is called crystals. When polymers fall into these crystalline arrangements, they give off heat. So the drop in the heat flow as a big dip in the plot of heat flow versus temperature is observed on DSC plot. This temperature is known as polymer's crystallization temperature or T_c.

Melting: If the polymer is further heated after T_c, eventually it will reach another thermal transition, called melting. When we reach the polymer's melting temperature, or T_m, those polymer crystals begin to fall apart, that is they melt. The chains come out of their ordered arrangements and begin to move around freely. There is a latent heat of melting as well as a latent heat of crystallization.

For present work, DSC analysis was carried out by means of modulated DSC (TA Instr. Model- 2910) in the temperature range 30 °C to 200 °C at a predetermined heating rate of 10 °C/min for pristine and irradiated samples at UGC-DAE-CSR, Indore.

2.3.7 UV-Vis Spectroscopy

Ultraviolet and visible (UV-Vis) absorption spectroscopy is the measurement of the attenuation of a beam of light after it passes through a sample or after reflection from a sample surface. Absorption measurements can be at a single wavelength or over an extended spectral range. Ultraviolet and visible light are energetic enough to promote outer electrons to higher energy levels. UV-Vis spectroscopy is usually applied to molecules or inorganic complexes in solution. The concentration of an analyst in solution can be determined by measuring the absorbance at some wavelength and applying the Beer-Lambert Law,

$$A = -log_{10}(I/I_0) = \varepsilon cL \qquad (2.3.21)$$

where A is the measured absorbance, I_0 is the intensity of the incident light at a given wavelength, I is the transmitted intensity, L the path length through the sample, and c the concentration of the absorbing specie. Different molecules absorb radiation of different wavelengths. An absorption spectrum will show a number of absorption bands corresponding to structural groups within the molecule. In a molecule, the atoms can rotate and vibrate with respect to each other. These vibrations and rotations

also have discrete energy levels, which can be considered as being packed on top of each electronic level.

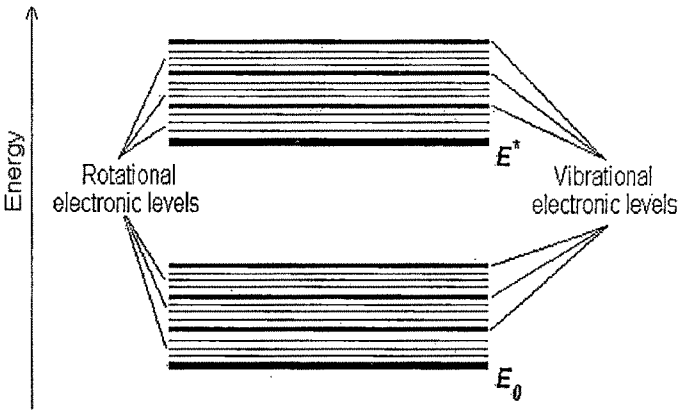

Fig.2.15 Electronic levels in energy absorption

Ultraviolet (UV) and Visible (Vis) light can cause electronic transitions. When a molecule absorbs UV-VIS radiation, the absorbed energy excites an electron into an empty, higher energy orbital. The absorbance of energy can be plotted against the wavelength to yield a UV-Vis spectrum. Most organic compounds that absorb UV-Vis radiation contain conjugated pi-bonds. Both the shape of the peak(s) and the wavelength of maximum absorbance (λ_{max}) give information about the structure of the compound.

Ultraviolet radiation has wavelengths of 200-400 nm. Visible light has wavelengths of 400-800 nm. The dual-beam design simultaneously measure absorption/transmittance coefficient spectrum of the sample and reference cells. Most spectrometers use a mirrored rotating chopper wheel to alternately direct the light beam through the sample and reference cells. The detection electronics or software program can then manipulate this coefficient values as the wavelength scans to produce the spectrum of absorbance or transmittance as a function of wavelength.

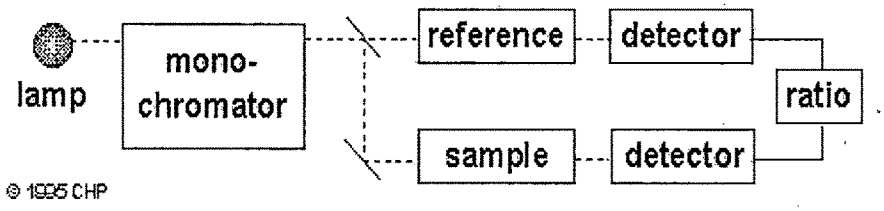

Fig. 2.16 Schematic of a dual-beam UV-Vis spectrophotometer

It measures the intensity of light passing through a sample (I), and compares it to the intensity of light before it passes through the sample (I_o). The ratio I / I_o is called the *transmittance*, and is usually expressed as a percentage (%T). The absorbance, A, is based on the transmittance

$$A = -\log(\%T)$$

Irradiation of polymeric materials results in the shifting of absorption edge from UV towards the visible region. This shift can be correlated with the optical band gap (Eg) using Tauc's expression [31].

$$\omega^2 \varepsilon_2(\lambda) = (h\omega - Eg)^2 \qquad (2.3.22)$$

where, $\varepsilon_2(\lambda)$ is the imaginary part of the complex refractive index, i.e., the optical absorbance and λ is the wavelength. Eg is usually derived from the plot $\varepsilon_2(\lambda)$ versus $1/\lambda$. The intersection of the extrapolated spectrum with abscissa yields the gap wavelength (λg), from which gap energy can be derived by

$$Eg = \frac{hc}{\lambda g} \qquad (2.3.23)$$

Optical characteristic of the pristine and irradiated samples have been studied in wavelength range of 250-900 nm by using U-3000/U-3300 Spectrophotometer (Hitachi) at IUAC, New Delhi.

2.3.8 Magnetic Properties

(i) Magnetic Force Microscope (MFM)

MFM is a scanning probe microscope (SPM) that can map the spatial distribution of magnetism by measuring the magnetic interaction between a sample and a tip. As magnetic devices have become smaller and smaller, an evaluation technique with nanoscale spatial resolution has become necessary. To meet this need, the MFM was developed. MFM is simply speaking, an AFM in which the tip can sense magnetic forces [32, 33].

The principle of MFM measurement is based on noncontact atomic force microscopy (NC-AFM). Unlike NC-AFM, magnetic materials are also used for the sample and tip, so that not only the atomic force but also the magnetic interactions are detected. Many kinds of magnetic interactions are measured by MFM, including magnetic dipolar interaction.

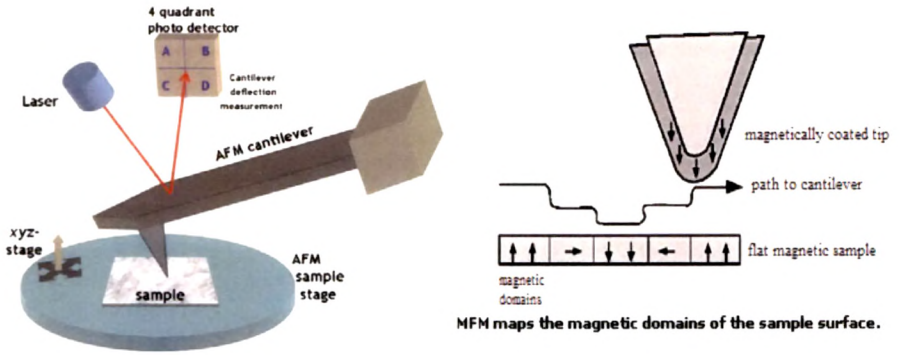

Fig. 2.17 working principle of MFM

The typical dimensions are a cantilever length of 200 μm, a tip length of 4 μm, a diameter of 50 nm and a distance from the surface is ~30 nm. The force on the magnetic tip (coated with ferromagnetic material) is detected by measuring the displacement of the end of the cantilever, usually by optical means. The forces measured in typical MFM applications are of the order of 30 pN, with typical

cantilever deflections of the order of nanometers. An image of the magnetic stray field is obtained by slowly scanning the cantilever over the sample surface, in a raster-like fashion. Typical scan areas are from 1 to 200 μm with imaging times of the order of 5-30 minutes.

Fig. 2.17 shows the most common layout of MFM. The peizo tube displaces the sample in the x and y directions in order to build, point by point, an image. The tip sits at the end of a flexible cantilever, which is part of larger chip that can be manipulated. Forces on the tip affect the position of the cantilever, whose instantaneous position is measured by reflection of a laser beam onto a position-sensitive detector.

One of the reasons for the widespread use of MFM is its ability to image surfaces that are not flat on the nanometer scale. In that case, separation of magnetic forces from varying atomic forces due to topography requires some care. A simple procedure consists in measuring first the topographic profile for each scan line. For that the tip moves at a constant height above the surface. The magnetic signal is measured on the second pass, in which the topographic signal is close to constant if the lift height is large enough [34].

For present work, MFM images were taken in 1x1 μm^2 area using Digital Nanoscope IIIa Instrument Inc. It gives the information about the magnetic domain formed on the surface of the sample in terms of phase shift.

(ii) SQUID (Superconducting Quantum Interference Device)

A superconducting quantum interference device (SQUID) is the most sensitive available device for measuring magnetic fields. Based on this, sensitive device called 'SQUID magnetometers' have been developed. SQUID magnetometers are used to characterize materials when the highest detection sensitivity over a broad temperature

range and using applied magnetic fields up to several Tesla is needed. High sensitivity is needed when samples with low intrinsic magnetic moment or low mass are measured. In thin films, for instance, the mass may be smaller than 1 microgram. These materials are therefore difficult to characterize using extraction or vibrating sample magnetometer but not with a SQUID magnetometer. Also for measurements of magnetic viscosity in permanent magnets, where small changes of magnetization as a function of time must be recorded, SQUID magnetometer is the best choice.

The SQUID consists of two superconductors separated by thin insulating layers to form two parallel Josephson junctions (Fig. 2.18(a)). The device may be configured as a magnetometer to detect incredibly small magnetic fields. In the superconductors on both sides of a Josephson junction, each of the Cooper pairs act as a single boson, defined by a single quantum-mechanical wave function. The wave functions do not go immediately to zero at the insulating barrier, however, if the barrier is thin enough, wave functions overlap, forming a single, continuous wave function that allows cooper pairs to tunnel through the junction.

This tunnelling makes the insulating barrier a weak superconductor, with the maximum or "critical" current, dependent on the temperature, the material, and the size of the junction.

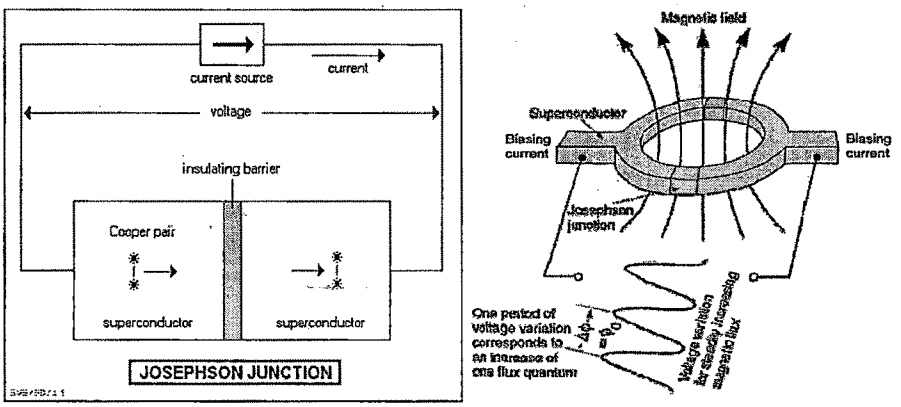

Fig. 2.18 (a) Josephson Junciton formation and (b) Principle of SQUID

To be useful, the output of a SQUID sensor has to be amplified and coupled to a measurement system. SQUID is useful to perform fundamental physical measurements, ranging from simple measurements of magnetic fields in material samples to detect the tiny displacements of large masses used in gravitational-wave detectors.

In present case, SQUID analysis of pristine and irradiated PI+Fe films was done to study the irradiation effect on the magnetic property for an applied field of 10KOrsted.

References

[1] D. Fink, M. Behar, V. Hnatowicz "Fundamentals of Ion-Irradiated Polymers" eds. D. Fink, Springer, Berlin, Heidelberg, New York,2004.

[2] Anjum Qureshi, N. L. Singh, A. K. Rakshit, F. Singh, V. Ganesan, Nucl. Instrum. & Meth. B. 244 (2006) 235.

[3] Anjum Qureshi, N. L. Singh, A. K. Rakshit, D. K. Avasthi, V. Ganesan, Surf. And Coat. Tech. 201 (2007) 8225.

[4] V.V. Shivakumar, S. VenkataRaman, B. P. Ajith Kumar, D.K. Avasthi, D. Sarangi, R. Bhattacharya and A. Gupta, Proceeding of National Symposium on Vacuum Science and Technology, cp-19, 1997.

[5] Ph.D. Thesis-Shantanu Ghosh "Electronic sputtering of thin films" 2001, JNU, New Delhi.

[6] J. F. Ziegler, code SRIM-2006, The stopping range of ions in matter (IBM Research), New York, USA, 2006.

[7] I. M. Govil and H. S. Hans. J. of Mysore Univ. Section B 26 (1976) 23; I M Govil, H.S. Hans Proc. Indian Acad. Sci (Engg. Sci.) Vol 3 Pt. 3, (1980) 237-252.

[8] NSC School on Accelerator Physics, NSC, 1989.

[9] R.H. BOYD, "*Methods* in *Experimental Physics*", Ed. R. A. Fava (Academic Press Inc., New York, 1980) 16 Part-C.

[10] N. A. Ashby, N. Z. Engng, 6 (1951) 33.

[11] C. W. Stillwell, Crystal Chemistry, (Mc. Graw-Hill Book Company, Inc., New York, 1938) pp. 29, 225-239.

[12] H. Tertsch, Festigkeitserscheinungen der Kristalle, (Springer-Verlag, Vienna, 1949), pp. 171-257.

[13] B. W. Mott, Microindentation Hardness Testing, (BitterwortHs, London, 1966) pp. 9.

[14] D. J. Clinton and R. Morrell, Mater. Chem. Phys., 17 (1987) 461.

[15] F. Frohlich, P. Grau and W. Grellmann, Phys. Stat. Sol. (a) 42 (1977) 79.

[16] P. N. Kotru, A. K. Razdan, B. M. Wanklyn, J. Mater. Sci., 24 (1989) 793.

[17] C. Hays and E. G. Kendall, Metallography, 6 (1973) 275.

[18] K. J. Pratap and V. Haribabu, Bull. Mater. Sci., 2 (1980) 43.

[19] A. Charlesby, Radiat. Phys. Chem., 40 (1992) 117.

[20] F. J. Balta Calleja, Adv. Polym. Sci. 66 (1985) 117.

[21] G. R. Rao, L. Riester, and E. H. Lee, Mat. Res. Soc. Symp. Proc., 345 (1995) 363.

[22] B. W. Mott, Microindentation Hardness Testing, (BitterwortHs, London, 1966) pp. 9.

[23] X-ray diffraction procedures by H.P. Klug, L. E. Alexander, Mellon Institute, John Wiley & Sons-New York, Chapman & Hall ltd. London, 1954.

[24] P. Scherrer, Gottinger Nachrichten, 2 (1918) 98.

[25] Brian C. Smith, Fundamentals of Fourier Transform Infrared spectroscopy, CRC press, Boca Raton, 1996.

[26] A. Karbach, D. Drechsler: Atomic force microscopy – a powerful tool for industrial applications. Surface and Interface analysis 27 (1999) 401-409.

[27] G. K. Bar, G. F. Meyers: The application of atomic force microscopy to the characterization of industrial polymer materials. MRS Bull. 29 (2004) 464-470.

[28] G. Kaupp "Atomic Force Microscopy, Scanning Nearfield Optical Microscopy and Nanoscratching" Springer, Berlin, Heidelberg, New York,2006.

[29] Rudolf Reichelt. "Science of Microscopy" vol.I, Eds. P. W. Hawkes, John C. H. Spence, Springer Science & Business Media, New York, 2007.

[30] Practical-DSC, Department of polymeric materials CTH, course: Polymeric material advance course, pp 1-6).

[31] J. Tauc, R. Grigorovici, A. Vancu, Phys. Stat. Sol. 15 (1966) 627.

[32] Y. Martin, H. K. Wickramasinghe, Appl. Phys. Lett. 50 (1987) 1455.

[33] J. J. Saenz, N. Garcia, P. Gruetter, E. Meyer, H. Heinzelmann, R. Wisendanger, L. Rosenthaler, H. R. Hidber, H. J.Guentherodt, J. Appl. Phys. 62 (1987) 4293.

[34] A. Thiaville, J. Miltat, J.M.Garcia, L. Abelmann, A. van den Bos, C. Lodder "Magnetic Microscopy of Nanostructures" eds. H. Hopster, H. P. Oepen, Springer, Berlin, Heidelberg, New York,2005.